CHEMISTRY
A European Journal

A Journal of
ChemPubSoc Europe

Accepted Article

Title: Control of Spatially Homogeneous Distribution of Heteroatoms to Produce Red TiO2 Photocatalyst for Visible-Light Photocatalytic Water Splitting

Authors: Xingxing Hong, Jun Tan, Huaze Zhu, Ningdong Feng, Yongqiang Yang, John Irvine, Lianzhou Wang, Gang Liu, and Hui-Ming Cheng

To be cited as: *Chem. Eur. J.* 10.1002/chem.201805283

Link to VoR: http://dx.doi.org/10.1002/chem.201805283

Supported by
ACES

WILEY-VCH

WILEY-VCH

DOI: 10.1002/((please add manuscript number))
Article type: Full Paper

Control of Spatially Homogeneous Distribution of Heteroatoms to Produce Red TiO_2 Photocatalyst for Visible-Light Photocatalytic Water Splitting

Xingxing Hong, Jun Tan, Huaze Zhu, Ningdong Feng, Yongqiang Yang, John T.S. Irvine, Lianzhou Wang, Gang Liu, Hui-Ming Cheng*

X. X. Hong, Prof. J. Tan, H. Z. Zhu, Dr. Y. Q. Yang, Prof. G. Liu, Prof. H. M. Cheng
Shenyang National Laboratory for Materials Science, Institute of Metal Research, Chinese Academy of Sciences, 72 Wenhua Road, Shenyang 110016, China

X. X. Hong, Prof. G. Liu
School of Materials Science and Engineering, University of Science and Technology of China, 72 Wenhua Road, Shenyang 110016, China

Dr N. D. Feng
State Key Laboratory of Magnetic Resonance and Atomic Molecular Physics, Wuhan Center for Magnetic Resonance, Key Laboratory of Magnetic Resonance in Biological Systems, Wuhan Institute of Physics and Mathematics, Chinese Academy of Sciences, Wuhan 430071, China

Prof. J. T.S. Irvine
School of Chemistry, University of St. Andrews, Fife, KY16 9ST, UK

Prof. L. Z. Wang
Nanomaterials Centre, School of Chemical Engineering and AIBN, The University of Queensland, St Lucia, Brisbane, QLD 4072, Australia

Prof. H. M. Cheng
Tsinghua-Berkeley Shenzhen Institute, Tsinghua University, 1001 Xueyuan Road, Shenzhen 518055, China

E-mail: gangliu@imr.ac.cn (GL)

Keywords: Titanium Dioxide; Photocatalysis; Homogeneous Doping; Water Splititng; Visible Light

10.1002/chem.201805283

WILEY-VCH

Abstract

The strong band-to-band absorption of photocatalysts spanning the whole visible light region (400-700 nm) is critically important for solar-driven photocatalysis. Although it is actively and widely used as photocatalyst for various reactions in the past four decades, TiO_2 has a very poor ability to capture the whole-spectrum visible light. Here, by controlling the spatially homogeneous distribution of boron and nitrogen heteroatoms in anatase TiO_2 microspheres with a predominance of high-energy {001} facets, a strong visible light absorption spectrum with a sharp edge beyond 680 nm is achieved. The red TiO_2 with the homogeneous doping of boron and nitrogen obtained shows no increase in defects like Ti^{3+} that are commonly observed in doped TiO_2. More importantly, it has the ability to induce photocatalytic water oxidation to produce oxygen under the irradiation of visible light beyond 550 nm and also photocatalytic reducing water to produce hydrogen under visible light. These results demonstrate the great promise of using the red TiO_2 for visible light photocatalytic water splitting and also provide an attractive strategy for realizing the wide-spectrum visible light absorption of wide-bandgap oxide photocatalysts.

Introduction

Inspired by natural photosynthesis proceeding in plants and some organisms that captures sunlight and converts it into chemical energy in the form of chemical bonds, photocatalysis, namely artificial photosynthesis, has been developed to induce different redox reactions for the applications that range from energy,[1-9] environment[10,11] to chemical synthesis[12,13] fields. Photocatalysis has three distinct steps, namely light absorption, separation of photogenerated charge carriers and catalysis reaction.[14,15] Among them the light absorption is the prerequisite step. In order to fully make use of solar light with around 45% visible light and also meet energetic requirement for water splitting (theoretical 1.23 eV plus several hundreds meV overpotential[16-18]), stable semiconductors with a bandgap of around 2 eV are the appropriate promising light absorbers for solar-driven photocatalysis. However, only a limited number of semiconducting materials are available for stable visible light photocatalysis under solar light. Besides the search for new semiconductors with suitable bandgaps,[19-23] various electronic structure modifiers (dopants,[24-28] defects,[20,29-33] strain[34] and disordering[35,36]) have been used to narrow the bandgap of various wide-bandgap oxide semiconductors for a wide spectrum absorption in visible light region. Although numerous studies on doped binary photocatalysts, particularly doped TiO_2, have been conducted,[37-39] the reported cases of realizing the desirable band-to-band redshift of the absorption edge in TiO_2 powder are still rare.[40-42] In this study, a semiconducting red TiO_2 photocatalyst with the strong band-to-band visible light absorption spectrum beyond 680 nm was achieved by controlling the homogeneous distribution of boron/nitrogen heteroatoms in the faceted TiO_2 microspheres. Moreover, as a result of the wide-spectrum absorption and also no increase in intrinsic defects, the red TiO_2 used as photocatalyst gives the ability to oxidize water to release oxygen under the irradiation of visible light with its wavelength longer than 550 nm, and to reduce water for hydrogen generation under visible light. These results could not only pave the pathway of

using modified TiO_2 photocatalyst for solar-driven water splitting but also provide a possible powerful strategy of extending the light absorption range of other wide-bandgap oxide photocatalysts.

Results and Discussion

Challenge of realizing homogeneous doping in TiO_2. The spatial distribution of electronic structure modifiers in materials has been identified as an important factor of determining the optical absorption modes of modified wide-bandgap semiconductors at atomic level.[30,33,36,38,43] The realization of a desirable band-to-band redshift of the absorption spectrum towards low-energy region by narrowing the bandgap intrinsically requires the homogeneous distribution of the modifiers in the whole bulk of materials while surface doping only generates an additional shoulder-like absorption band in the low-energy region by forming some localized states in the gap. Developing the capability of controlling the spatial distribution of dopants in non-layered metal oxides is, therefore, highly necessary and remains a challenge. One feasible strategy relying on thermodynamic consideration is to locally weaken strong chemical bonds in the bulk for an easy substitutional doping. A preliminary attempt in this aspect was that,[42] by conducting the nitrogenation in a gaseous ammonia atmosphere to anatase TiO_2 microspheres with a concentration gradient of boron dopant that can effectively weaken the surrounding Ti-O bonds, a concentration gradient of B/N dopants was formed to induce an additional strong visible light absorption band (Figure 1c of **ref. 42**). Unfortunately, this co-doped TiO_2 as *particulate* photocatalyst for water splitting under visible light showed little activity largely because the concentration gradient of dopants cannot cause the full mergence of the electronic states of B/N dopants with original valence band of TiO_2 for a satisfactory bulk transport of charge carriers.

The challenge of achieving the desirable homogeneous B/N doping in TiO_2 by the above strategy is intrinsically restricted by the feature that the interstitial boron atoms with a small

ionic diameter in bulk tend to migrate towards the surface layer of the TiO_2 microspheres and finally concentrate in the surface layer when subject to thermal treatment at high temperature,[44] as demonstrated in **Figure S1**. Pristine boron doped TiO_2 microspheres used in this study, which were synthesized from the acidic hydrolysis of TiB_2 at hydrothermal condition, have a relatively uniform dispersion of boron dopant in the bulk (**Figure S2**). Thermal treatment at 600 ^oC in air leads to the formation of a concentration gradient of interstitial boron with the maximum at the surface (Figure S1a). In contrast, the depth profiles (Figure S1b) of XPS B 1*s* spectra of boron doped TiO_2 after the thermal treatment at a relatively low temperature 460 ^oC suggest the retained uniform dispersion of both the interstitial boron (its binding energy, around 191 eV) and substitutional boron (its binding energy, around 188 eV) for lattice oxygen in the bulk. Therefore, to address the challenge, developing effective low-temperature nitrogenation routes, in which the migration of boron dopant from bulk to surface of materials is avoided, is crucial. In addition, it should be pointed out that thermodynamically metastable substitutional boron in TiO_2 tends to convert into the stable interstitial boron when subject to the high temperature thermal treatment.[45]

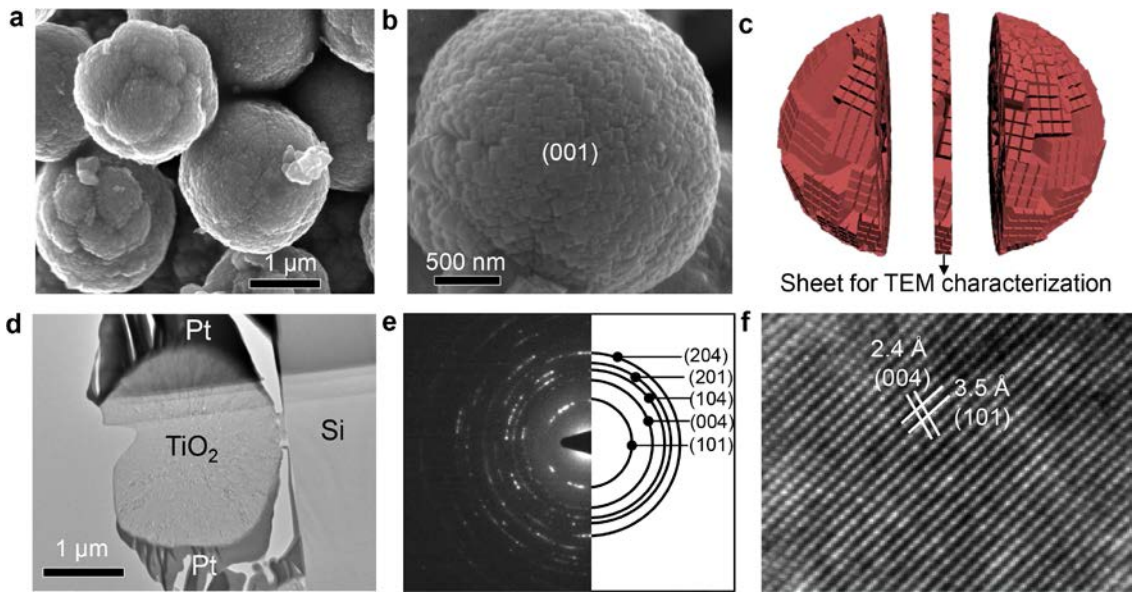

Figure 1 Morphology and microstructures of the TiO_2 microspheres with the homogeneous B/N doping. **a** and **b,** SEM images of the B/N doped TiO_2 microspheres. **c**, Schematic of

cutting one sphere of the doped TiO_2 dispersed on a silicon substrate by Focused Ion Beam technique. The middle thin sheet was used for TEM characterization. **d**, TEM image of the sheet cut from the sphere that was adhered on the silicon substrate by depositing a platinum layer on the exposed surface of the sphere. **e**, Electron diffraction patterns indexed to anatase TiO_2 recorded from the sheet of doped TiO_2 in **d**. **f**, High resolution TEM image obtained from a typical region of the sheet in **d**.

Low-temperature nitrogenation-induced homogeneous B/N doping. Different from the widely used conventional nitrogenation process that uses gaseous ammonia as nitrogen source and is usually performed at the temperature of over 600 ^oC for a heavy nitrogen doping, urea (CH_4N_2O) was chosen as solid nitrogen source in the low-temperature (as low as 460 ^oC) nitrogenation process developed in this study. During the nitrogenation, the urea was placed separately from the sample of TiO_2 microspheres with well dispersed boron dopant in bulk, as shown in **Figure S3**. The reason for choosing urea as nitrogen source lies in that the thermal decomposition of urea in an inert atmosphere can occur at the temperature as low as 200 ^oC and complete at 450 ^oC, accompanying the release of gaseous products including NH_3 and HNCO for nitrogen doping.[46] Moreover, HNCO species and its derivatives released from urea is considered to play a crucial role in realizing homogeneous B/N doping in this study, to be validated in the following sections.

Comparison of X-ray diffraction patterns of boron doped TiO_2 microspheres before and after nitrogen doping shows no obvious change in crystal structure (**Figure S4**). Morphology and microstructure of the homogeneous B/N doped TiO_2 microspheres were investigated by scanning electron microscopy (SEM) and transmission electron microscopy (TEM). Comparison of SEM images of pristine boron doped TiO_2 microspheres (**Figure S5**) and TiO_2 microspheres with the homogeneous B/N doping (**Figure 1a**) suggests the good retaining of the basic morphology of particles due to the low-temperature nitrogenation. The sharp edges

and flat surfaces of the {001} facets-terminated squares with the size of tens of nanometers, which contribute to the surface of the microspheres, are clearly observed in **Figure 1b**. In contrast, the surface of the microspheres with a concentration gradient of B/N prepared at 600 ^{o}C in an NH_3 atmosphere (Figure 1a of ref. 42) was rough, probably because of the high-temperature corrosion in the reductive atmosphere.

To directly investigate the microstructures and spatial distribution of composition of the TiO_2 microspheres with the homogeneous B/N doping, a thin sheet with its thickness suitable for TEM characterization was cut from one microsphere along its diameter direction, as illustrated in **Figure 1c**. The relatively uniform contrast of the TEM image in **Figure 1d** (also see the TEM image with a higher magnification in **Figure S6**) suggests that the building blocks in the sheet share some crystallographic orientation, largely the [001] direction, because the microsphere surface is terminated with {001} facets. This feature is supported by selective area electron diffraction patterns of the sheet in **Figure 1e**, where no complete diffraction rings are formed. High resolution TEM image in **Figure 1f** shows clear lattice fringes with the spacings of 2.4 and 3.5 Å that are assigned to (001) and (101) planes of anatase TiO_2. The similar ionic diameter of nitrogen to oxygen together with the mild nitrogenation process is responsible for the high crystallinity of the homogeneous boron/nitrogen doped TiO_2 microspheres. The high crystallinity facilitates the transport of photogenerated charge carriers.

The homogeneous distribution of nitrogen and boron in the microspheres together with their chemical states was revealed by the combination of energy dispersive X-ray spectroscopy (EDS) and X-ray photoelectron spectroscopy (XPS). The EDS elemental maps of Ti-K, O-K and N-K in **Figure 2b-d**, recorded from the sheet in **Figure 2a**, show the uniform spatial distribution of nitrogen dopant in the whole sheet. The similar intensity change trend of the radial line-scan profiles of N-K to O-K in **Figure 2e** further verifies the uniformity of nitrogen dopant in the sheet. XPS spectrum of N 1*s* from pristine surface of the

B/N doped microspheres in **Figure 2f** gives two strong signals at 397.8 and 399.6 eV. The less changed intensity of the former and rapidly decreased intensity of the latter in the depth profiles of N 1*s* XPS spectra suggest their location in bulk and surface of the microspheres, respectively. On the basis of the binding energy, the former can be definitely assigned to the substitutional nitrogen for lattice oxygen in the form of Ti-N bonds.[24] The atomic ratio of the substitutional N to Ti at different depths of the microspheres has a small fluctuation between 3.5 at% and 4.8 at% (**Figure 2g**), again suggesting the homogeneous distribution of the substitutional nitrogen in the microspheres. In addition, the good dispersion of boron dopant in the microspheres is retained after nitrogen doping, as indicated by the depth dependent XPS spectra of B 1*s* in **Figure S7**. Moreover, comparison of nuclear magnetic resonance spectra (**Figure S8**) of environment and amount of boron in TiO_2 keeps unchanged before and after nitrogen doping.[47]

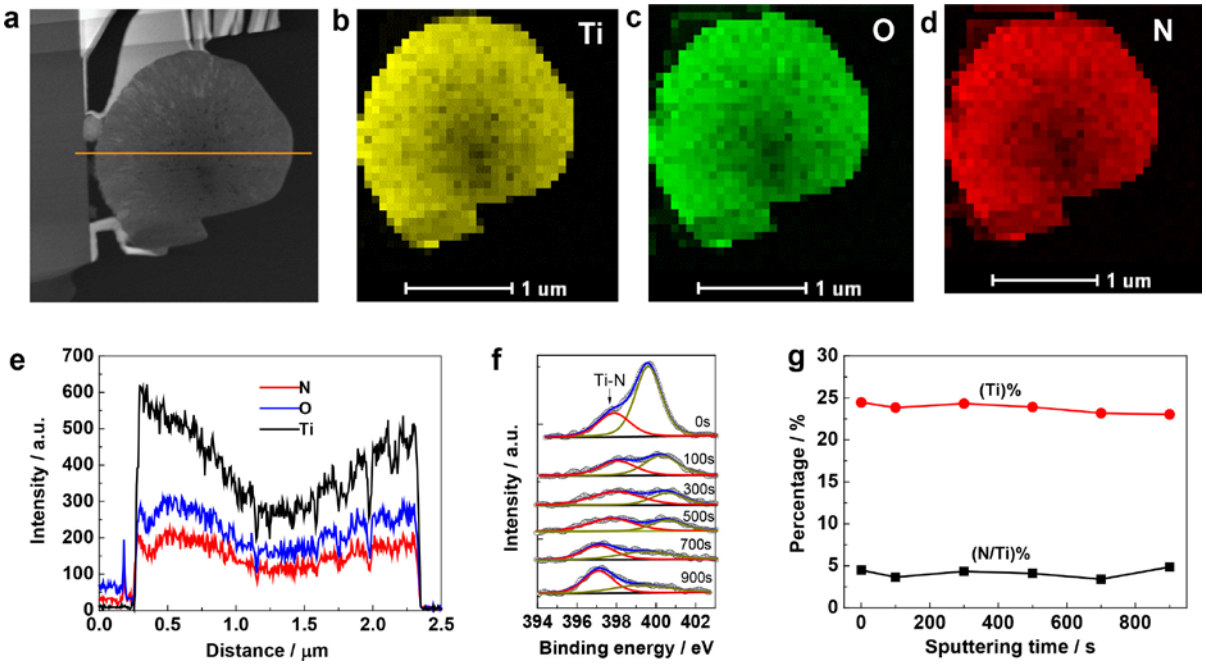

Figure 2 Homogeneous distribution and chemical state of nitrogen in the TiO_2 microspheres with the homogeneous B/N doping. **a-d,** Scanning TEM high angle annular dark field (STEM-HAADF) image and EDS elemental mapping images of Ti-K, O-K and N-K recorded from the sheet in Fig. 2a. **e**, Line-scan profiles of Ti-K, O-K and N-K along the orange line in

Fig. 2a. **f**, Depth profiles of XPS spectrum of N 1*s* recorded from the TiO_2 microspheres with the homogeneous B/N doping as a function of Ar^+ sputtering time. **g**, Atomic percentage of Ti and atomic ratio of N to Ti in the TiO_2 microspheres with the homogeneous B/N doping as a function of Ar^+ sputtering time.

The identity of the 399.6 eV signal in N 1*s* XPS spectrum is the adsorbate containing nitrogen anion, likely associated with HNCO and/or its derivatives released from the thermal decomposition of urea, as detected by Fourier transform infrared spectroscopy (FTIR). Comparison of the FTIR spectra (**Figure S9**) of two different boron/nitrogen doped TiO_2 samples, which were prepared at the same conditions but with NH_3 and urea as nitrogen source, respectively, demonstrates the presence of an additional weak band with two peaks at around 2079 and 2020 cm^{-1} in the sample prepared with urea as nitrogen source. A similar 2073 cm^{-1} band was proposed to be anionic CH_2CN species on metal oxides.[48] Such adsorbates on the microspheres are considered to play an important role in driving the effective diffusion of nitrogen species from the surface into bulk for homogeneous nitrogen doping at a relatively low-temperature. Typical doping process by heating a solid sample in a gaseous atmosphere containing dopant species (like nitrogen doping in an ammonia atmosphere) requires the adsorption and dissociation of dopant molecules on sample surface, and diffusion of active dopant species in the sample bulk. There is a strong compromise between the adsorption and the dissociation and diffusion of active species upon heating temperatures. A low heating temperature favors dopant molecule adsorption but not for dissociation of molecules and diffusion of active dopant species in the bulk. The strong interaction between the adsorbate and TiO_2 is confirmed by the fact that the adsorbate can stand up to a 600 ^oC heating in an argon atmosphere (**Figure S10**). This feature greatly facilitates the diffusion of nitrogen dopant towards the bulk. In addition, the stability of these

adsorbates is further indicated by the good retaining of the signal in the FTIR spectra after exposure to the light irradiation in air or in reaction solution (**Figure S11**).

Homogeneous B/N doping-induced band-to-band visible light absorption band. On the basis of the above results, the nitrogenation with urea as nitrogen source at 460 ^{o}C resulted in the homogeneous B/N doping in the TiO_2 microspheres, as schematically shown in the top panel of **Figure 3a**. As a result, the absorption edge of the doped TiO_2 with a red color has a great red-shift by 286 nm and spans the whole visible light range in **Figure 3b**. The extraordinary red-shift of the whole absorption edge suggests band-to-band photon excitations of a narrowed bandgap. The bandgap is narrowed to be 1.97 eV determined by extrapolating the plot with a steep edge of the transformed Kubelka–Munk function versus the light energy in **Figure S12**. The origin of the bandgap narrowing observed is attributed to the elevated maximum of O 2*p* states-dominated valence band with the involvement of N 2*p* states, as fully investigated theoretically in literature.[24]

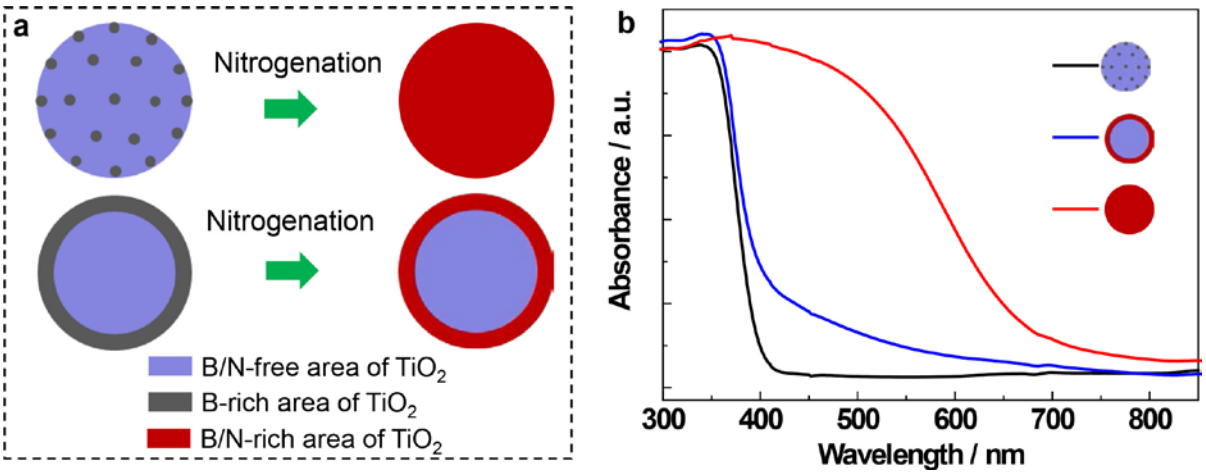

Figure 3 Effect of the spatial distribution of boron and nitrogen in TiO_2 on their absorption spectra. **a**, Schematic of the doped TiO_2 sample (the top panel) with homogeneous distribution of boron and nitrogen in the whole sphere, and (the bottom panel) with a gradient distribution of boron and nitrogen in the sphere shell. **b,** UV-visible absorption spectra of two doped TiO_2

samples with homogeneous distribution of boron and nitrogen, and with gradient distribution of boron and nitrogen in the shell, and pristine boron-doped TiO_2.

The formation of such an extraordinary visible light absorption band is sensitive to both the spatial distribution of boron dopant in the TiO_2 microspheres and nitrogen source used in the nitrogenation process. When boron dopant was concentrated in the surface layer of the microspheres as shown in the bottom panel of Figure 3a, the nitrogenation at the same conditions (urea as nitrogen source; heating temperature 460 ^oC) only caused the formation of an additional weak shoulder-like absorption band in visible light range in Figure 3b. On the other hand, the NH_3-assisted nitrogenation of the TiO_2 microspheres with well dispersed boron dopant in bulk also caused the formation of a weak shoulder-like absorption band (**Figure S13**) largely due to the poor diffusion ability of the nitrogen dopant from surface to bulk at 460 ^oC. Based on all these results, one can infer that the high dispersity of boron dopant (facilitating the substitutional doping of nitrogen for oxygen) and unique function of urea as nitrogen source (promoting the diffusion of nitrogen dopant into bulk by forming the adsorbate-containing nitrogen dopant on TiO_2) are responsible for the homogeneous nitrogen doping and thus band-to-band visible light absorption. The pictures of three B/N doped TiO_2 samples discussed here together with pristine B doped TiO_2 samples are given in **Figure S14**.

Defects and electrical conductivity of homogeneous B/N doped TiO_2. Defects, in particular oxygen vacancies and related Ti^{3+}, always exist in doped TiO_2 largely due to the charge imbalance with the introduction of dopants and loss of lattice oxygen in reductive atmosphere. They can affect photocatalytic activity of materials by changing transport of charge carriers and surface adsorption of reactants. Electron spin resonance (ESR) spectroscopy was used to detect the change of the type and amount of defects in the TiO_2 microspheres with well dispersed boron dopant before and after nitrogen doping. As shown in **Figure 4a**, no additional new defects were observed after nitrogen doping. More importantly,

the intensity of the original resonance signal at g = 1.9995 in boron doped TiO_2, typically assigned to oxygen vacancies,[49] is reversely lowered with the introduction of substitutional nitrogen dopant that has a more negative valence state than lattice oxygen (N^{3-} *vs* O^{2-}) and usually causes the generation of additional oxygen vacancies in common nitrogen-doped TiO_2. The reason for this different result is that the charge compensation between the interstitial boron B^{3+} and substitutional nitrogen N^{3-} can suppress the formation of new oxygen vacancies in the TiO_2 with homogeneous B/N doping. This means that the nitrogenation of the microspheres with well dispersed boron dopant does not lead to the formation of additional potential recombination centres of photogenerated charge carriers. The good retaining of semiconducting nature of the TiO_2 microspheres with homogeneous doping of boron and nitrogen is confirmed by the current-voltage curve measured from a microsphere connected with two tungsten probes. The curve in **Figure 4b** shows the typical feature of a metal-semiconductor junction with Schottky contact.

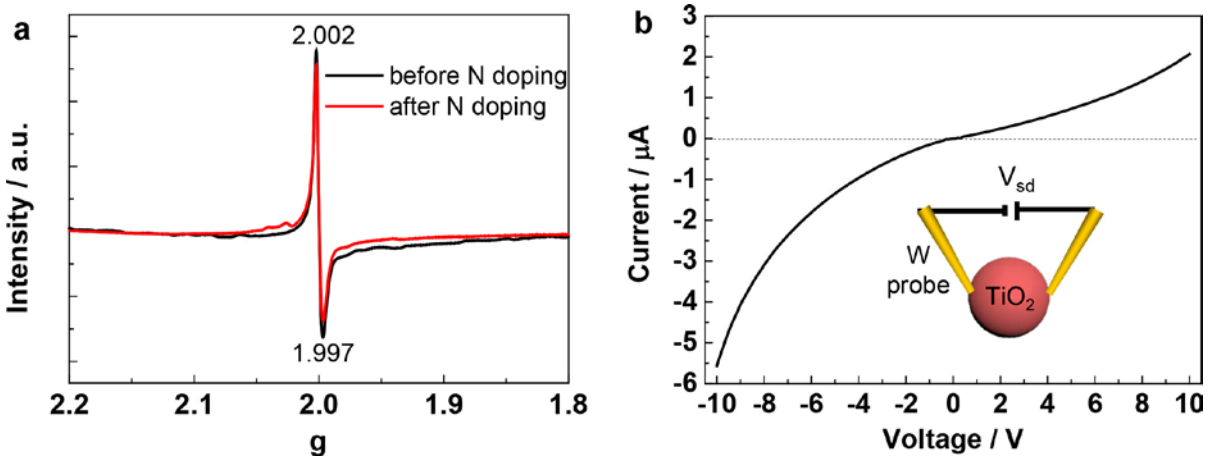

Figure 4 a, Electron spin resonance spectra of the TiO_2 microspheres with well dispersed boron dopant before and after nitrogen doping. The measured temperature was 140 K. **b**, Current-voltage curve measured from a B/N doped TiO_2 microsphere at room temperature. The inset is the schematic of measuring a microsphere with two tungsten probes, which was performed in a scanning electron microscope.

Photocatalytic water splitting. Photocatalytic activity of the homogeneous B/N doped TiO_2 (red TiO_2) was first estimated by conducting water oxidation half reaction under visible light. **Figure 5a** shows photocatalytic oxygen evolution activity of six cycling tests for 24 h. The red TiO_2 has the ability to continuously release oxygen from water oxidation with the rate of 36 μmol h^{-1} g^{-1} in the first cycle. The oxygen evolution activity has some decay after the first cycling test but keeps marginal fluctuations in the subsequent five cycles. The decay should be mainly caused by the deposition of Ag particles on photocatalyst surface from the reduction of Ag^+ as sacrificial agent by the photogenerated electrons in photocatalytic reaction. In all cycling tests, the release of nitrogen from the oxidation of nitrogen species in red TiO_2 photocatalyst by the photogenerated holes occurs, suggesting the photo-corrosion instability of bare red TiO_2. This is a common problem that most photocatalysts of nitrogen doped metal oxides, metal nitrides and also metal oxynitrides have[50]. Loading suitable oxidative co-catalysts is a general method to solve this problem. As shown in Figure 5b, RuO_2 modified red TiO_2 has the ability of completely suppressing the release of nitrogen. Moreover, the oxygen evolution rate is greatly improved from pristine 36 to 81.6 μmol h^{-1} g^{-1} after loading RuO_2 co-catalyst. The action spectrum obtained under monochromatic light with different wavelengths in **Figure 5c** shows that the red TiO_2 with the homogeneous B/N doping is active beyond 550 nm. These results further suggest that the oxygen generation indeed comes from photocatalytic reaction. On the contrary, the sample with boron dopant (white TiO_2) is inactive under visible light due to no visible light absorption, and another reference sample with a shoulder-like visible light absorption band (see the blue curve in Figure 3b) is also inactive largely due to the low absorbance and low mobility of photogenerated holes associated with the shoulder-like band. These results demonstrate the advantage of the band-to-band visible light absorption of the red TiO_2 obtained in inducing visible light photocatalytic water oxidation.

To further evaluate the potential applicability of the developed red TiO_2 as a visible light responsive O_2 producing photocatalyst, its activity is directly compared with that of WO_3 and $BiVO_4$ that are two most widely studied visible light O_2 producing photocatalysts. As shown in **Figure S15**, the oxygen producing activity of the red TiO_2 microspheres under visible light is comparable with that of the faceted $BiVO_4$ crystals[51], and is much higher than that of two WO_3 based photocatalysts[52] after loading 1 wt% RuO_2 co-catalyst under the same measurement conditions. Considering the fact that the red TiO_2 microspheres have a comparable particle size with the $BiVO_4$ crystals and larger particle size than the WO_3 crystals used here (see SEM images in **Figure S16**), the wider absorption range of the red TiO_2 shall play an important role in contributing to its visible light activity. It should be pointed out that both WO_3 and $BiVO_4$ are inactive in producing H_2 because of their lower conduction band edges than the redox level of proton reduction.

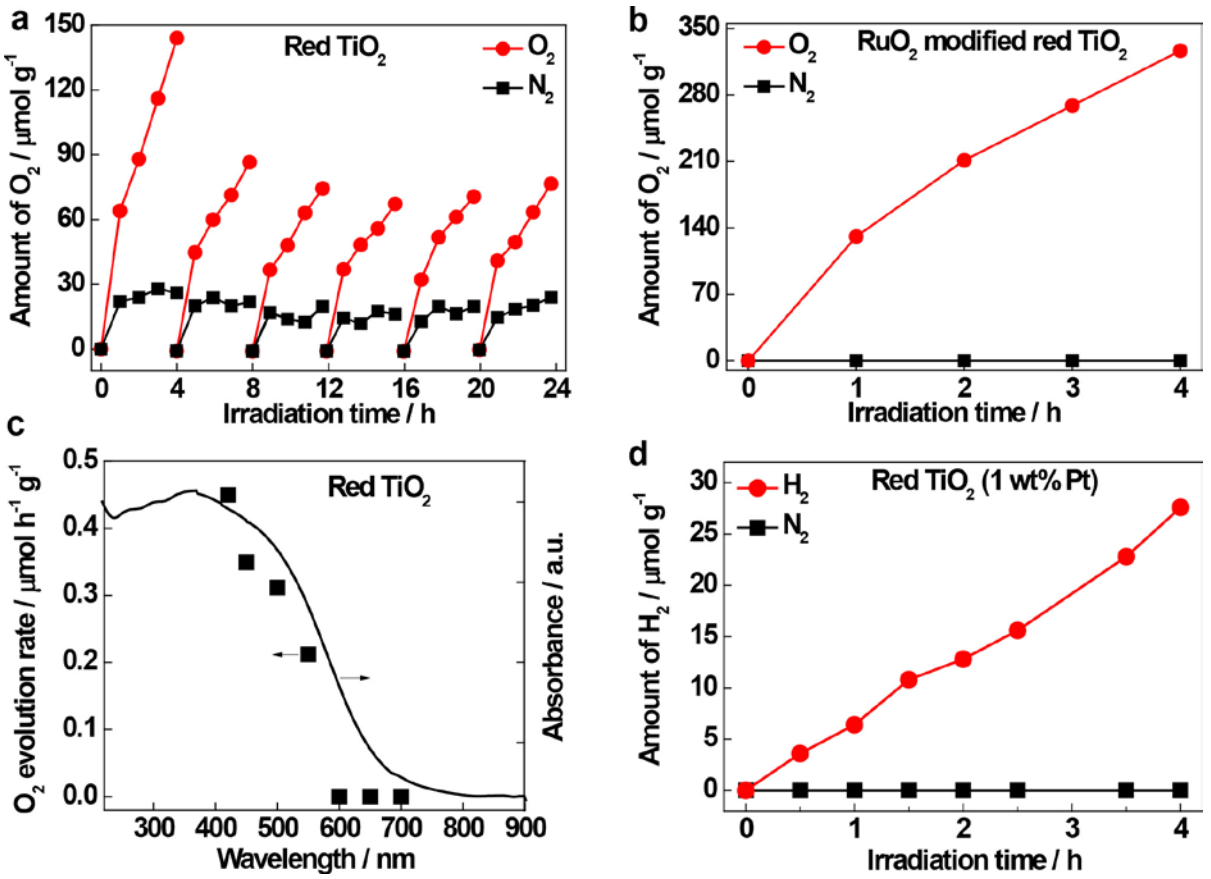

Figure 5 a, Cycling tests of photocatalytic oxygen generation from an aqueous solution of $AgNO_3$ by the TiO_2 microspheres with homogeneous B/N doping (red TiO_2) as a function of the exposure time to visible light. **b**, Photocatalytic oxygen generation from an aqueous solution of $AgNO_3$ by the red TiO_2 modified with 1 wt% RuO_2 co-catalyst as a function of the exposure time to visible light. The wavelength and intensity of incident light used in **a** and **b** is $\lambda > 420$ nm and 74.2 $mWcm^{-2}$. The release of nitrogen was also monitored in the tests of **a** and **b**. **c**, Photocatalytic oxygen generation from an aqueous solution of $AgNO_3$ by the red TiO_2 as a function of the wavelength of irradiation light. **d**, Photocatalytic hydrogen generation from an aqueous solution containing 10 vol% methanol as sacrificial agent by 0.5 wt% Pt loaded red TiO_2 with homogeneous B/N doping as a function of the exposure time to visible light (The wavelength and intensity of incident light, $\lambda > 420$ nm and 74.2 $mWcm^{-2}$). The evolution of nitrogen was also monitored.

Photocatalytic activity of the homogeneous B/N doped TiO_2 (red TiO_2) was further estimated by conducting water reduction half reaction in the presence of methanol as sacrificial agent under visible light. **Figure 5d** demonstrates a nearly linear increase of photocatalytic hydrogen evolution by 0.5 wt% Pt loaded red TiO_2 with the light irradiation time increase. Moreover, no any nitrogen was monitored in photocatalytic water reduction reaction. These results suggest the good stability of red TiO_2 as a photocatalyst for hydrogen evolution. It is useful to understand the underlying reason for the much lower photocatalytic hydrogen evolution rate of red TiO_2 than its oxygen evolution rate in the half reactions (6.9 versus 81.6 $\mu mol\ h^{-1}\ g^{-1}$). Similar trend was also observed in Ta_3N_5 photocatalyst[53]. The proposed reason for the low hydrogen evolution rate is the presence of the large Schottky barriers at the interfaces of the red TiO_2 microspheres and co-catalyst Pt particles with a larger work function that makes the transfer of the photogenerated electrons from red TiO_2 to Pt not sufficient[53-55]. In contrast, the upward surface band bending of n-type red TiO_2 facilitates the

transfer of the photogenerated holes from red TiO_2 to reactants. Further effort of solving the imbalance in photocatalytic hydrogen and oxygen generation is to reduce the barrier between red TiO_2 and the co-catalyst so that overall water splitting might be achieved by the modified red TiO_2 photocatalyst.

Conclusion

A novel nitrogenation route was developed to realize a desirable homogeneous boron and nitrogen doping in TiO_2 microspheres with {001} facets for a strong wide spectrum visible light absorption band. The success of this route is using urea as solid nitrogen source at the nitrogenation temperature as low as 460 ^oC. It was found that the adsorption of HNCO and related derivatives released from thermal hydrolysis of urea on TiO_2 surface greatly facilitates the diffusion of nitrogen dopant towards the bulk of the microspheres to induce homogeneous nitrogen doping with the assistance of boron dopant. The chemical state of nitrogen dopant was revealed as substitutional nitrogen for oxygen. As a consequence of the homogeneous boron and nitrogen doping, a strong band-to-band absorption spanning the whole visible light range was achieved. The resultant red TiO_2 microspheres have the ability to induce photocatalytic water oxidation for oxygen evolution under the irradiation of visible light with its wavelength beyond 550 nm and visible light photocatalytic water reduction for hydrogen evolution, indicating that TiO_2 can be used as building blocks to construct solar-driven photocatalysts for solar fuel generation.

Supporting Information

Supporting Information including sample preparation, characterization, processing the microsphere by a Focused Ion Beam, electrical conductivity measurement, photocatalytic water splitting measurements, is available from the Wiley Online Library or from the author.

Acknowledgements

The authors thank National Natural Science Fundation of China (Nos. 51825204, 51572266，21633009, 51629201), the Major Basic Research Program, Ministry of Science and Technology of China (2014CB239401), the Key Research Program of Frontier Sciences CAS (QYZDB-SSW-JSC039) for the financial support. G. L. is grateful for the award of the Newton Advanced Fellowship.

[1] A. Fujishima, K. Honda, *Nature*, **1972**, *238*, 37-+.

[2] K. Maeda, K. Teramura, D. L. Lu, T. Takata, N. Saito, Y. Inoue, K. Domen, *Nature*, **2006**, *440*, 295.

[3] S. Chen, T. Takata, K. Domen, *Nat. Rev. Mater.* **2017**, *2*, (10).

[4] S. Zhu, D. Wang, *Adv. Energy Mater.* **2017**, *7*, (23).

[5] W. Luo, Z. Yang, Z. Li, J. Zhang, J. Liu, Z. Zhao, Z. Wang, S. Yan, T. Yu, Z. Zou, *Energy & Environ. Sci.* **2011**, *4*, 4046-4051.

[6] F. Wen, C. Li, *Acc. Chem. Res.* **2013**, *46*, 2355-2364.

[7] H. Li, J. Shang, Z. Ai, L. Zhang, *J. Am. Chem. Soc.* **2015**, *137*, 6393-6399.

[8] S.-I. Naya, T. Kume, R. Akashi, M. Fujishima, H. Tada, *J. Am. Chem. Soc.*, **2018**, *140*, 1251-1254.

[9] Y. Goto, T. Hisatomi, Q. Wang, T. Higashi, K. Ishikiriyama, T. Maeda, Y. Sakata, S. Okunaka, H. Tokudome, M. Katayama, S. Akiyama, H. Nishiyama, Y. Inoue, T. Takewaki, T. Setoyama, T. Minegishi, T. Takata, T. Yamada, K. Domen, *Joule* **2018**, *2*, 509-520.

[10] M. R. Hoffmann, S. T. Martin, W. Y. Choi, D. W. Bahnemann, *Chem. Rev.* **1995**, *95*, 69-96.

[11] C. Chen, W. Ma, J. Zhao, *Chem. Soc. Rev.* **2010**, *39*, 4206-4219.

[12] X. Lang, X. Chen, J. Zhao, *Chem. Soc. Rev.* **2014**, *43*, 473-486.

[13] J. Kou, C. Lu, J. Wang, Y. Chen, Z. Xu, R. S. Varma, *Chem. Rev.* **2017**, *117*, 1445-1514.

[14] A. L. Linsebigler, G. Q. Lu, J. T. Yates, *Chem. Rev.* **1995**, *95*, 735-758.

[15] J. Yang, D. Wang, H. Han, C. Li, *Acc. Chem. Res.* **2013**, *46*, 1900-1909.

[16] A. Grimaud, O. Diaz-Morales, B. Han, W. T. Hong, Y.-L. Lee, L. Giordano, K. A. Stoerzinger, M. T. M. Koper, Y. Shao-Horn, *Nat. Chem.* **2017**, *9*, 457-465.

[17] L. C. Seitz, C. F. Dickens, K. Nishio, Y. Hikita, J. Montoya, A. Doyle, C. Kirk, A. Vojvodic, H. Y. Hwang, J. K. Norskov, T. F. Jaramillo, *Science* **2016**, *353*, 1011-1014.

[18] J. Suntivich, K. J. May, H. A. Gasteiger, J. B. Goodenough, Y. Shao-Horn, *Science* **2011**, *334*, 1383-1385.

[19] X. Wang, K. Maeda, A. Thomas, K. Takanabe, G. Xin, J. M. Carlsson, K. Domen, M. Antonietti, *Nat. Mater.* **2009**, *8*, 76 -80.

[20] X. Xu, C. Randorn, P. Efstathiou, J. T. S. Irvine, *Nat. Mater.* **2012**, *11*, 595 -598.

[21] M. L. Lv, X. Q. Sun, S. H. Wei, C. Shen, Y. L. Mi, X. X. Xu, *ACS Nano,* **2017**, *11*, 11441 -11448.

[22] R. Kuriki, T. Ichibha, K. Hongo, D. Lu, R. Maezono, H. Kageyama, O. Ishitani, K. Oka, K. Maeda, *J. Am. Chem. Soc.* **2018**, *140*, 6648-6655.

[23] X. Zhu, T. Zhang, Z. Sun, H. Chen, J. Guan, X. Chen, H. Ji, P. Du, S. Yang, *Adv. Mater.* **2017**, *29*, (17).

[24] R. Asahi, T. Morikawa, T. Ohwaki, K. Aoki, Y. Taga, *Science* **2001**, *293*, 269-271.

[25] W. Zhao, W. H. Ma, C. C. Chen, J. C. Zhao, Z. G. Shuai, *J. Am. Chem. Soc.* **2004**, *126*, 4782-4783.

[26] a) V. Gombac, L. De Rogatis, A. Gasparotto, G. Vicario, T. Montini, D. Barreca, G. Balducci, P. Fornasiero, E. Tondello, M. Graziani, *Chem. Phys.* **2007**, *339*, 111-123; b) S. In, A. Orlov, R. Berg, F. Garcia, S. Pedrosa-Jimenez, M. S. Tikhov, D. S. Wright, R. M. Lambert, *J. Am. Chem. Soc.* **2007**, *129*, 13790–13791. c) G. Liu, Y. N. Zhao, C. H. Sun, F. Li, G. Q. Lu, H. M. Cheng, *Angew. Chem. Int. Ed.* **2008**, *47*, 4516-4520.

[27] A. Loiudice, J. Ma, W. S. Drisdell, T. M. Mattox, J. K. Cooper, T. Thao, C. Giannini, J. Yano, L.-W. Wang, I. D. Sharp, R. Buonsanti, *Adv. Mater.* **2015**, *27*, 6733-+.

[28] Q. Sun, D. Cortie, S. Zhang, T. J. Frankcombe, G. She, J. Gao, L. R. Sheppard, W. Hu, H. Chen, S. Zhuo, D. Chen, R. L. Withers, G. Mcintyre, D. Yu, W. Shi, Y. Liu, *Adv. Mater.* **2017**, *29*, (11).

[29] I. Nakamura, N. Negishi, S. Kutsuna, T. Ihara, S. Sugihara and E. Takeuchi, *J. Mol. Catal. a-Chem.* **2000**, *161*, 205-212.

[30] P. Niu, L.-C. Yin, Y.-Q. Yang, G. Liu and H.-M. Cheng, *Adv. Mater.* **2014**, *26*, 8046-8052.

[31] H. Li, J. Li, Z. Ai, F. Jia, L. Zhang, *Angew. Chem. Int. Ed.* **2018**, *57*, 122-138.

[32] F. Zuo, K. Bozhilov, R. J. Dillon, L. Wang, P. Smith, X. Zhao, C. Bardeen, P. Feng, *Angew. Chem. Int. Ed.* **2012**, *51*, 6223-6226.

[33] Y. Yang, L.-C. Yin, Y. Gong, P. Niu, J.-Q. Wang, L. Gu, X. Chen, G. Liu, L. Wang, H.-M. Cheng, *Adv. Mater.* **2018**, *30* (6).

[34] S. L. Wang, X. Luo, X. Zhou, Y. Zhu, X. Chi, W. Chen, K. Wu, Z. Liu, S. Y. Quek, G. Q. Xu, *J. Am. Chem. Soc.* **2017**, *139*, 15414 -15419.

[35] X. Chen, L. Liu, P. Y. Yu, S. S. Mao, *Science* **2011**, *331*, 746-750.

[36] Y. Kang, Y. Yang, L.-C. Yin, X. Kang, G. Liu, H.-M. Cheng, *Adv. Mater.* **2015**, *27*, 4572-4577.

[37] M. Anpo, M. Takeuchi, *Catal.* **2003**, *216*, 505-516.

[38] G. Liu, L. Wang, H. G. Yang, H.-M. Cheng, G. Q. Lu, *J. Mater. Chem.* **2010**, *20*, 831-843.

[39] M. Kapilashrami, Y. Zhang, Y.-S. Liu, A. Hagfeldt, J. Guo, *Chem. Rev.* **2014**, *114*, 9662-9707.

[40] M. Kitano, K. Funatsu, M. Matsuoka, M. Ueshima, M. Anpo, *J. Phys. Chem. B* **2006**, *110*, 25266-25272.

[41] G. Liu, C. Sun, L. Wang, S. C. Smith, G. Q. Lu, H.-M. Cheng, *J. Mater. Chem.* **2011**, *21*, 14672 -14679.

[42] G. Liu, L.-C. Yin, J. Wang, P. Niu, C. Zhen, Y. Xie, H.-M. Cheng, *Energy Environ. Sci.* **2012**, *5*, 9603 -9610.

[43] G. Liu, L. Wang, C. Sun, X. Yan, X. Wang, Z. Chen, S. C. Smith, H.-M. Cheng, G. Q. Lu, *Chem. Mater.* **2009**, *21*, 1266-1274.

[44] G. Liu, J. Pan, L. Yin, J. T. S. Irvine, F. Li, J. Tan, P. Wormald and H.-M. Cheng, *Adv. Funct. Mater.* **2012**, *22*, 3233 -3238.

[45] E. Finazzi, C. Di Valentin and G. Pacchioni, *J. Phys. Chem. C* **2009**, *113*, 220-228.

[46] P. A. Schaber, J. Colson, S. Higgins, D. Thielen, B. Anspach and J. Brauer, *Thermochimica Acta* **2004**, *424*, 131 -142.

[47] N. Feng, A. Zheng, Q. Wang, P. Ren, X. Gao, S.-B. Liu, Z. Shen, T. Chen and F. Deng, J. *Phys. Chem. C* **2011**, *115*, 2709-2719.

[48] C. C. Chuang, W. C. Wu, M. X. Lee, J. L. Lin, *Phys. Chem. Chem. Phys.* **2000**, *2*, 3877-3882.

[49] Y. Nakaoka, Y. Nosaka, *Photochem. Photobio. a-Chem.* 1997, *110*, 299-305.

[50] A. Kudo and Y. Miseki, *Chem. Soc. Rev.* **2009**, *38*, 253-278.

[51] R. G. Li, F. X. Zhang, D. Wang, J. X. Yang, M. R. Li, J. Zhu, X. Zhou, H. X. Han, C. Li, *Nat. Commun.* **2012**, *4*, 1432.

[52] Y. P. Xie, G. Liu, L. C. Yin, H. M. Cheng, *J. Mater. Chem.* 2012, *22*, 6746-6751.

[53] D. Wang, T. Hisatomi, T. Takata, C. S. Pan, M. Katayama, J. Kubota, K. Domen, *Angew. Chem. Int. Ed.* **2013**, *52*, 11252-11256.

[54] G. Liu, L. Ma, L. C. Yin, G. D. Wan, H. Z. Zhu, C. Zhen, Y. Q. Yang, Y. Liang, J. Tan, H. M. Cheng, *Joule* **2018**, *2*, 1095-1107.

[55] G. Liu, L. C. Yin, J. Pan, F. Li, L. Wen, C. Zhen, H. M. Cheng, *Adv. Mater.* **2015**, *27*, 3507-3512.

Received: ((will be filled in by the editorial staff))
Revised: ((will be filled in by the editorial staff))
Published online: ((will be filled in by the editorial staff))

10.1002/chem.201805283

WILEY-VCH

Table of contents

By controlling spatially homogeneous distribution of boron and nitrogen heteroatoms in faceted anatase TiO_2 microspheres, an extraordinary strong band-to-band visible light absorption spectrum with the sharp absorption edge was achieved. The resultant red anatase TiO_2 can induce photocatalytic water oxidation and reduction under visible light.

Keyword: Titanium Dioxide, Photocatalysis, Homogeneous Doping, Water Splitting, Visible Light

X. X. Hong, J. Tan, H. Z. Zhu, N. D. Feng, Y. Q. Yang, J. TS Irvine, L. Z. Wang, G. Liu,* H.-M. Cheng

Title: Control of Spatially Homogeneous Distribution of Heteroatoms to Produce Red TiO_2 Photocatalyst for Visible-Light Photocatalytic Water Splitting